Study of Boron–Nitrogen Dative Bonds using Azetidine Inversion Dynamics

Cam Thuy Hoang, Ivan Prokes, Guy J. Clarkson, Matthew J. Rowland, James H. R. Tucker,* Michael Shipman,* and Tiffany R. Walsh*

[a] *Department of Chemistry, University of Warwick, Gibbet Hill Road, Coventry, CV4 7AL, UK. Fax: +44 2476 524112; Tel: +44 2476 523186; E-mail: m.shipman@warwick.ac.uk*

[b] *School of Chemistry, University of Birmingham, Edgbaston, Birmingham, B15 2TT, UK. Fax: +44 121 414 4403; E-mail: j.tucker@bham.ac.uk*

[c] *Institute for Frontier Materials, Deakin University, Waurn Ponds, 3216 VIC, Australia. Tel: +61 352 273 116; E-mail: tiffany.walsh@deakin.edu.au*

Supplementary Information

3,3-Dimethyl-1-(phenylmethyl)azetidine 1. To a solution of 1-(*p*-toluenesulfonyl)-3,3-dimethylazetidine (**5**)[1] (396 mg, 1.65 mmol) in methanol (5 mL) was added magnesium powder (282 mg, 11.6 mmol). The mixture was sonicated for 2 h, then diluted with Et_2O (3 mL) and $Na_2SO_4.10H_2O$ (854 mg, 2.65 mmol) added. After stirring for a further 30 minutes, the mixture was filtered. Oxalic acid (75 mg, 0.83 mmol) dissolved in a minimal amount of EtOH was added to the filtrate. The solvent was removed *in vacuo* to give 3,3-dimethylazetidine oxalate salt (121 mg) as a white solid. This material was redissolved in CH_2Cl_2 (5 mL) and anhydrous Et_3N (0.13 mL, 0.93 mmol). The mixture was stirred for 30 minutes then benzaldehyde (0.05 mL, 0.47 mmol) was added. The reaction was stirred at room temperature for 12 h before addition of sodium triacetoxyborohydride (164 mg, 0.78 mmol). The mixture was stirred for a further 6 h, then quenched with saturated aqueous Na_2CO_3 solution and extracted with CH_2Cl_2. The combined organic layers were dried over Na_2SO_4, filtered and concentrated *in vacuo*. Purification on basic alumina (CH_2Cl_2 → CH_2Cl_2/MeOH 90/10) afforded **1** (49 mg, 34% over 2 steps) as a yellow oil. IR (film) 3660, 2956, 2872, 1627, 1450 cm^{-1}; ^1H NMR (400 MHz, $CDCl_3$) δ 1.14 (s, 6H), 2.91 (s, 4H), 3.54 (s, 2H), 7.09-7.30 (m, 5H); ^{13}C NMR (100 MHz, $CDCl_3$) δ 27.5 (CH_3), 31.6 (C), 63.8 (CH_2Ph), 66.8 (CH_2 azetidine), 126.8 (CH), 128.2 (2 x CH), 128.4 (2 x CH), 138.6 (C); HRMS (ESI) calculated for $C_{12}H_{18}N$ [M+H]: 176.1434, found: 176.1434.

2-(3,3-Dimethyl-1-azetidinylmethyl)phenylboronic acid (6). To a solution of 1-(*p*-toluenesulfonyl)-3,3-dimethylazetidine (**5**)[1] (821 mg, 3.44 mmol) in methanol (10 mL) was added magnesium powder (584 mg, 24 mmol). The reaction was sonicated for 3 h then diluted with Et_2O (5 mL) and $Na_2SO_4.10H_2O$ (1.77 g, 5.5 mmol) added. After stirring for a further 30 minutes, the mixture was filtered. Oxalic acid (155 mg, 1.72 mmol) dissolved in a minimal amount of EtOH was added to the filtrate. The solvent was removed *in vacuo* to give 3,3-dimethylazetidine oxalate salt (314 mg) as a white solid. This material was redissolved in CH_2Cl_2 (10 mL) and anhydrous Et_3N (0.34 mL, 2.42 mmol). The mixture was stirred for 30 minutes then 2-formylphenylboronic acid (181 mg, 1.21 mmol) was added. The reaction was stirred at room temperature for 12 h before addition of sodium triacetoxyborohydride (408 mg, 1.93 mmol). The mixture was stirred for a further 6 h, then quenched with saturated aqueous Na_2CO_3 solution and extracted with CH_2Cl_2. The combined organic layers were dried over Na_2SO_4, filtered and concentrated *in vacuo*. Purification on basic alumina (EtOAc → EtOAc/MeOH 90/10) afforded **6** (180 mg, 48% over 2 steps) as a white solid. M.p. 184

°C. IR (film) 3676, 2953, 2813, 1599, 1447 cm^{-1}. ^{1}H NMR (400 MHz, CDCl$_3$) δ 1.09 (s, 6H), 1.20 (br s, 2H), 3.29 (s, 4H), 4.16 (s, 2H), 7.03-7.27 (m, 3H), 7.60 (d, *J* = 5.4 Hz, 1H). ^{13}C NMR (100 MHz, CDCl$_3$) δ 27.7 (CH$_3$), 29.6 (C), 64.7 (CH$_2$Ph), 64.9 (CH$_2$ azetidine), 124.3 (CH), 126.5 (CH), 127.2 (CH), 131.9 (CH), 141.2 (2 x C). ^{11}B NMR (160 MHz, CDCl$_3$) δ 14.1 (64%), 23.1 (36%). HRMS (ESI) calculated for $C_{12}H_{19}BNO_2$ [*M*+H]: 220.1506, found: 220.1501.

2-(3,3-Dimethyl-1-azetidinylmethyl)phenylcatechol boronate (3). Compound **6** (53 mg, 0.24 mmol) and catechol (27 mg, 0.24 mmol) were dissolved in CHCl$_3$ (3 mL) and stirred with MgSO$_4$ (500 mg) at room temperature for 30 minutes. The mixture was filtered then concentrated *in vacuo* to give **3** as a white solid (70 mg, 99%). IR (film) 3676, 2956, 2927, 1600, 1482 cm^{-1}. ^{1}H NMR (400 MHz, CDCl$_3$) δ 1.05 (s, 3H), 1.28 (s, 3H), 3.11 (d, *J* = 10.9 Hz, 2H), 3.87 (d, *J* = 10.9 Hz, 2H), 4.28 (s, 2H), 6.65-6.72 (m, 2H), 6.76-6.82 (m, 2H), 7.03-7.09 (m, 1H), 7.17-7.24 (m, 2H), 7.42-7.47 (m, 1H). ^{13}C NMR (125 MHz, CDCl$_3$) δ 26.1 (CH$_3$), 28.8 (C), 29.5 (CH$_3$), 65.7 (CH$_2$ azetidine), 66.6 (CH$_2$Ph), 109.7 (2 x CH), 119.4 (2 x CH), 122.7, 128.2, 128.6, 131.1, 139.4 (2 x C), 152.0 (2 x C). ^{11}B NMR (160 MHz, CDCl$_3$) δ 13.7. ^{11}B NMR (160 MHz, *d*$_2$-TCE) δ 13.6. ^{11}B NMR (160 MHz, *d*$_5$-pyridine) δ 14.1. HRMS (ESI) calculated for $C_{18}H_{21}BNO_2$ [*M*+H]: 294.1663, found: 294.1664.

2-(3,3-Dimethyl-1-azetidinylmethyl)phenylpinacol boronate (4). Compound **6** (48 mg, 0.22 mmol) and pinacol (26 mg, 0.22 mmol) were dissolved in benzene (3 mL) and stirred with molecular sieves (500 mg) at reflux for 12 h. The mixture was filtered then concentrated *in vacuo* to give **4** as a white solid (49 mg, 74%). IR (film) 3674, 2963, 1601, 1447 cm^{-1}. ^{1}H NMR (400 MHz, CDCl$_3$) δ 1.27 (s, 18H), 3.45 (s, 4H), 4.16 (s, 2H), 6.97 (d, *J* = 6.7 Hz, 1H), 7.05-7.16 (m, 2H), 7.47 (d, *J* = 6.7 Hz, 1H). ^{13}C NMR (100 MHz, CDCl$_3$) δ 26.1 (CH$_3$), 26.7 (CH$_3$), 28.5 (C), 63.8 (CH$_2$ azetidine), 65.5 (CH$_2$Ph), 79.2 (C), 122.1 (CH), 126.3 (2 x CH), 130.3 (CH), 138.5 (2 x C). ^{11}B NMR (160 MHz, CDCl$_3$) δ 13.7. ^{11}B NMR (160 MHz, CD$_2$Cl$_2$) δ 13.9. HRMS (ESI) calculated for $C_{18}H_{29}BNO_2$ [*M*+H]: 302.2289, found: 302.2280.

Compound **1**

^{1}H NMR

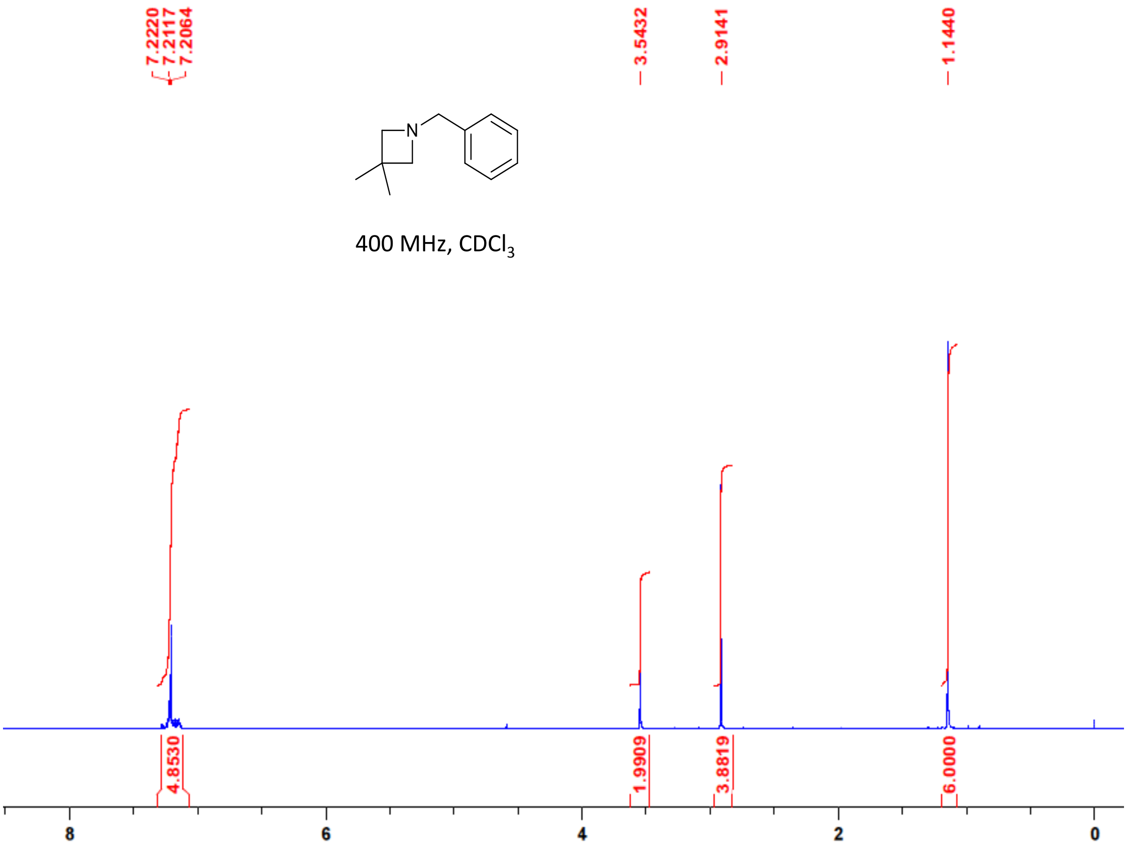

^{13}C NMR

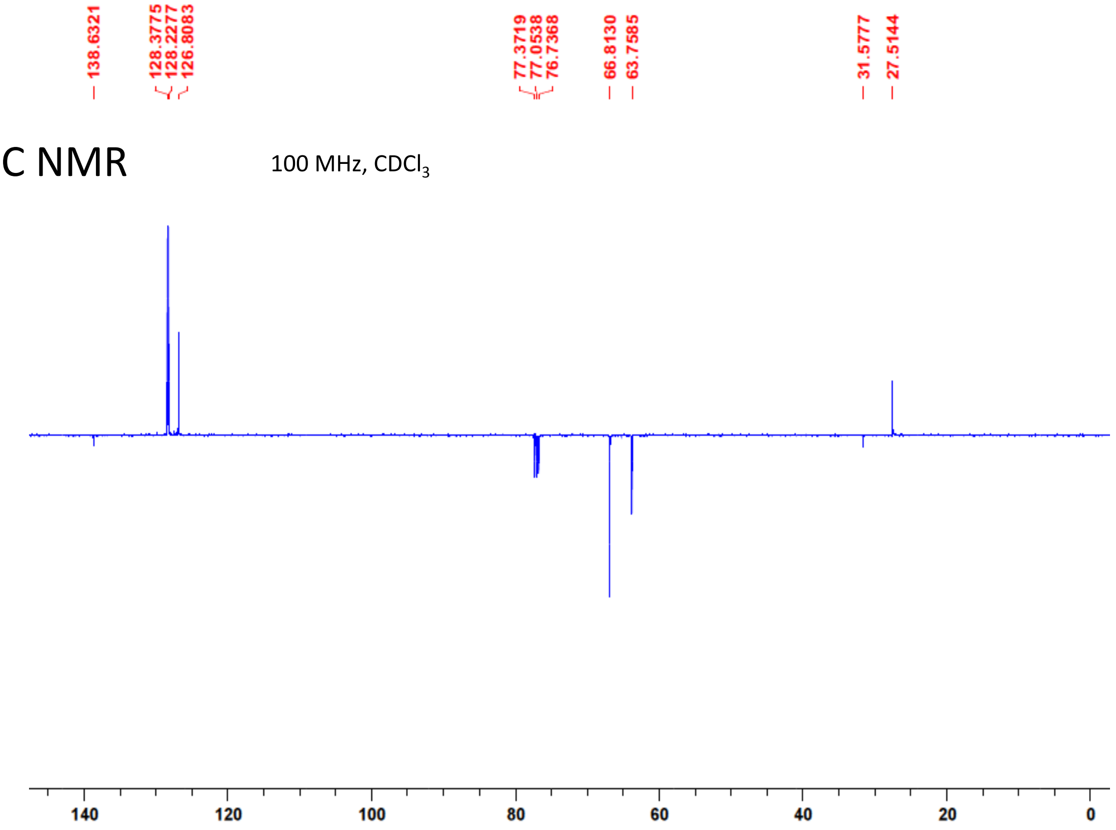

^{1}H NMR

Compound **6**

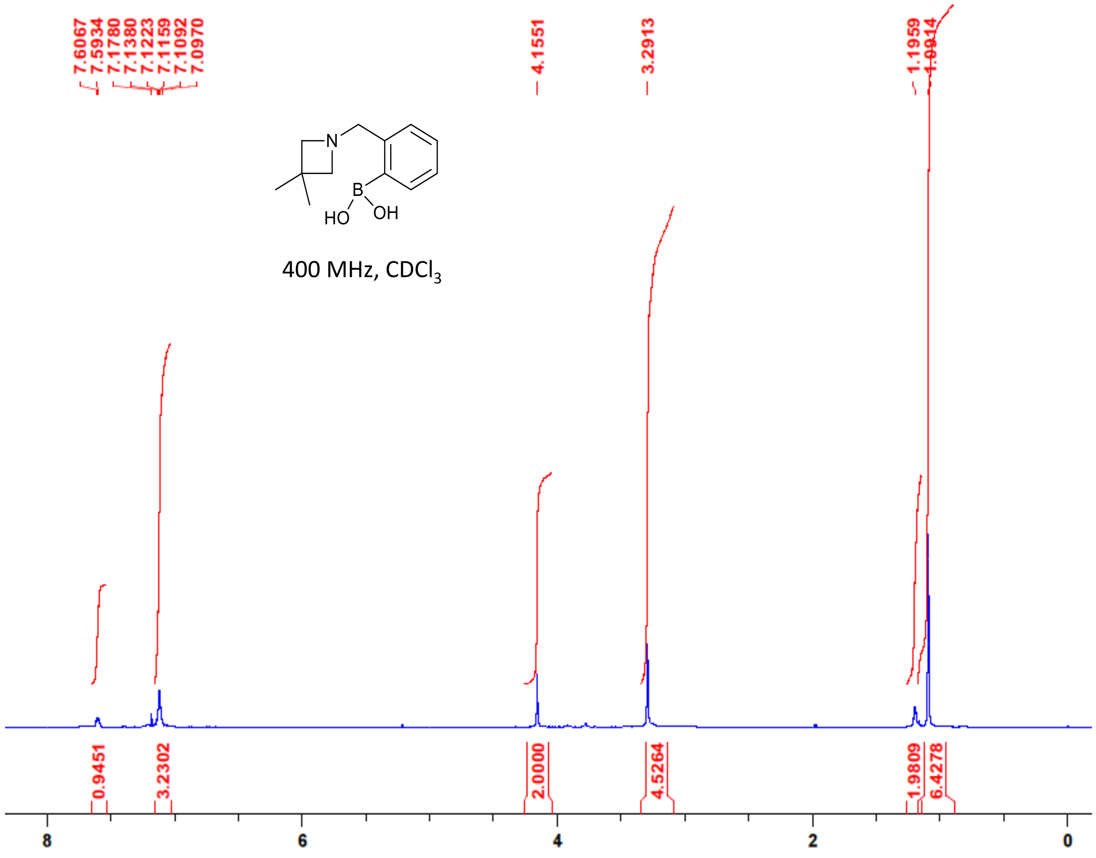

400 MHz, $CDCl_3$

^{13}C NMR

100 MHz, $CDCl_3$

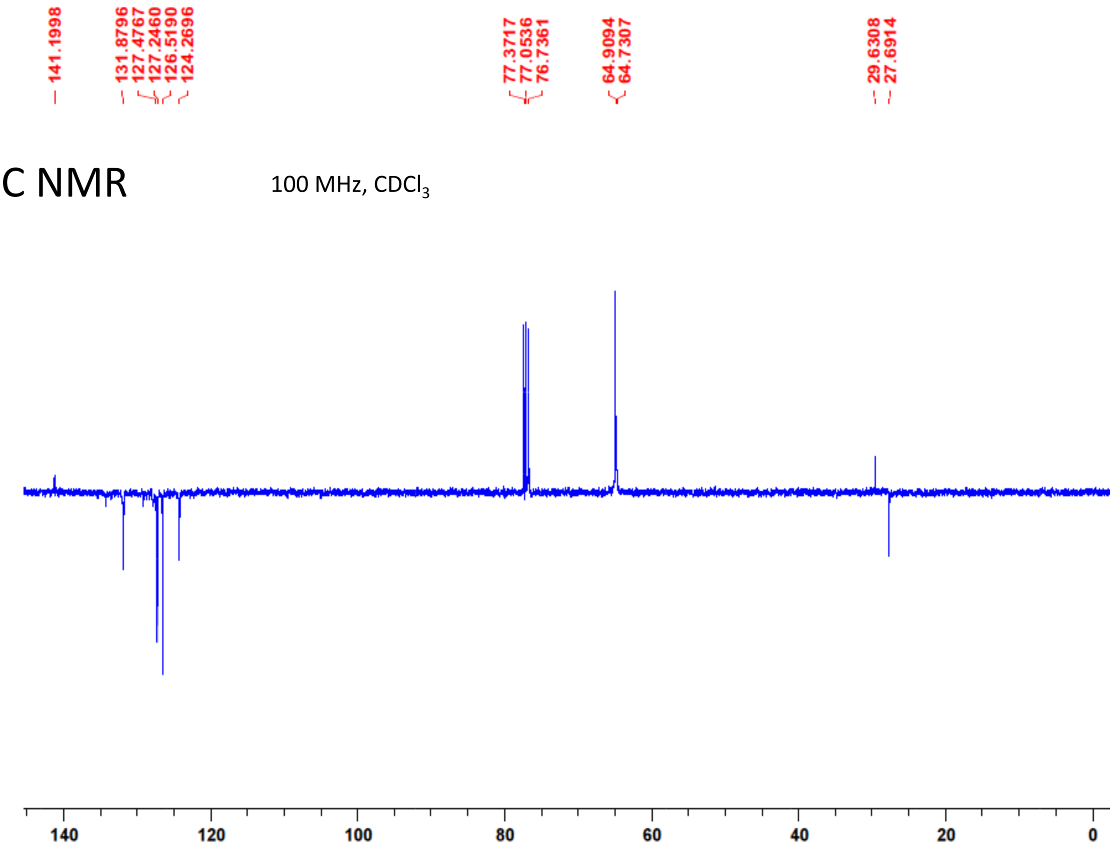

Compound **6**

^{11}B NMR

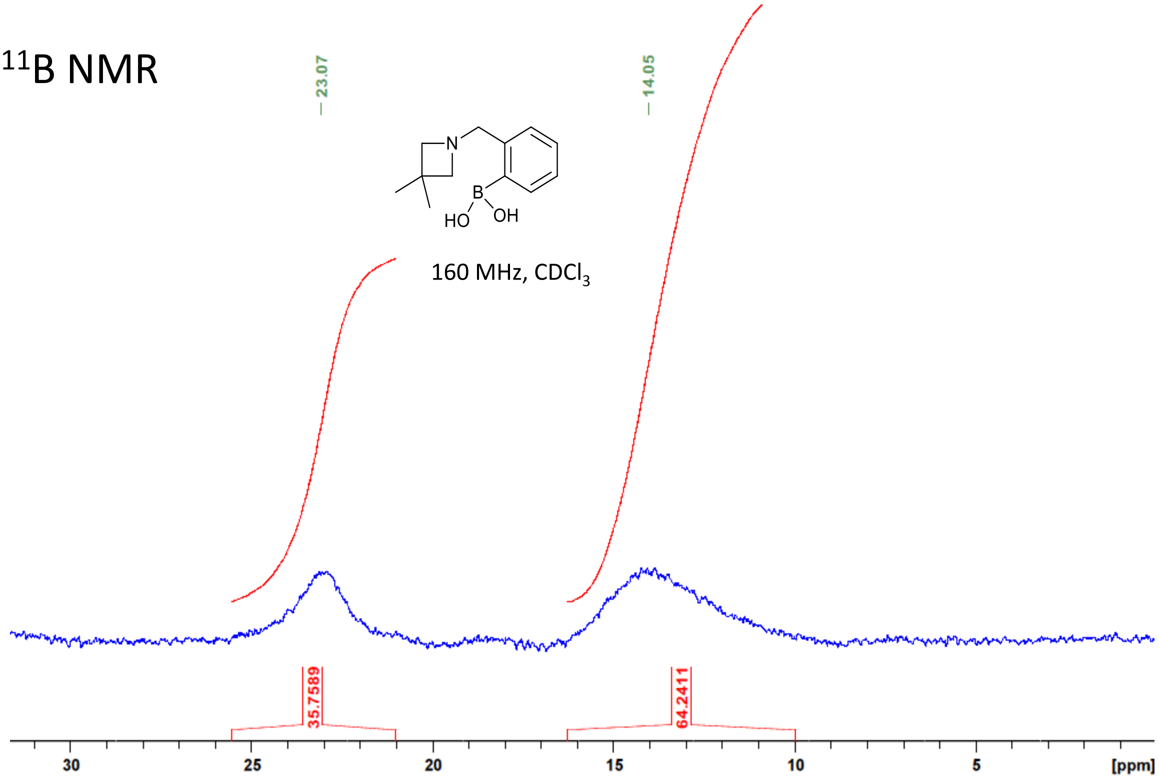

Compound **3**

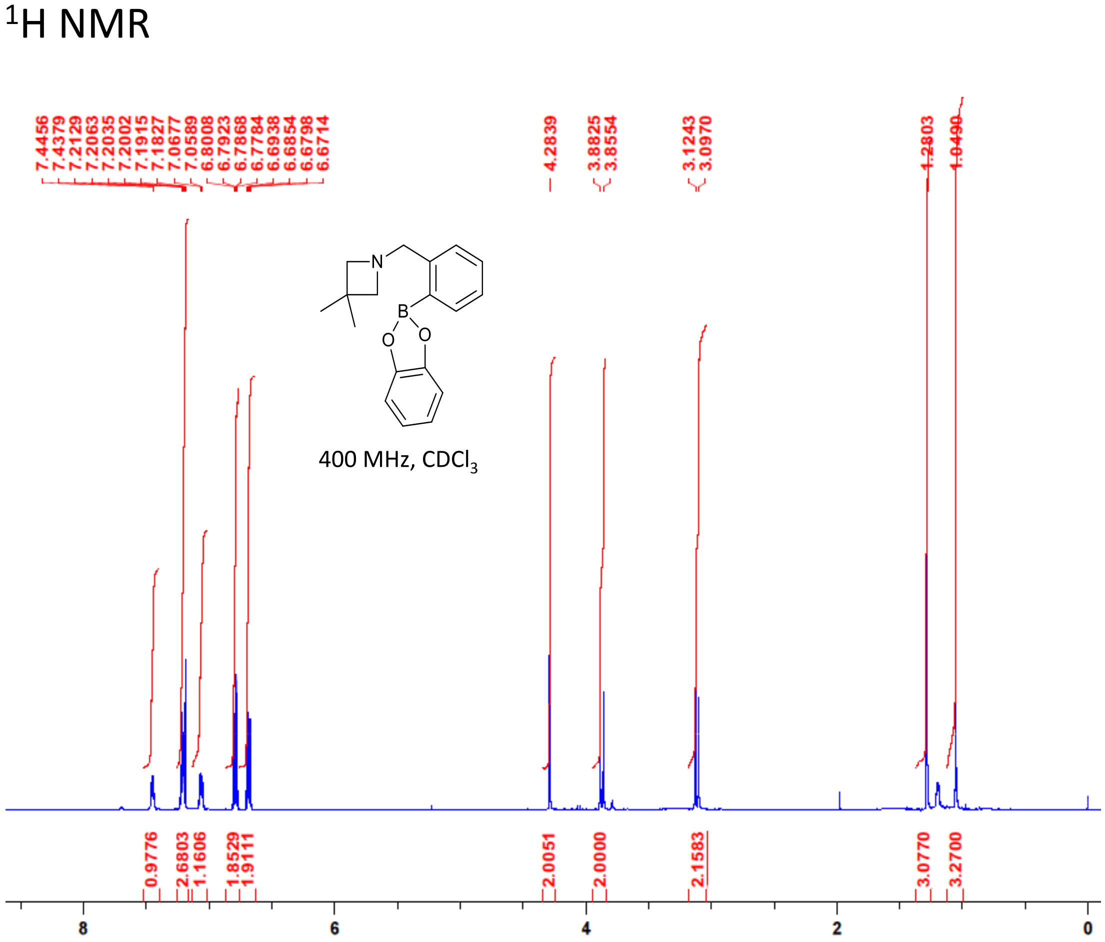
^{1}H NMR
7.4456
7.4379
7.2129
7.2063
7.2035
7.2002
7.1915
7.1827
7.0677
7.0589
6.8008
6.7923
6.7868
6.7784
6.6938
6.6854
6.6798
6.6714
4.2839
3.8825
3.8554
3.1243
3.0970
1.2803
1.0490
N
B
O
O
400 MHz, $CDCl_3$
0.9776
2.6803
1.1606
1.8529
1.9111
2.0051
2.0000
2.1583
3.0770
3.2700
8
6
4
2
0

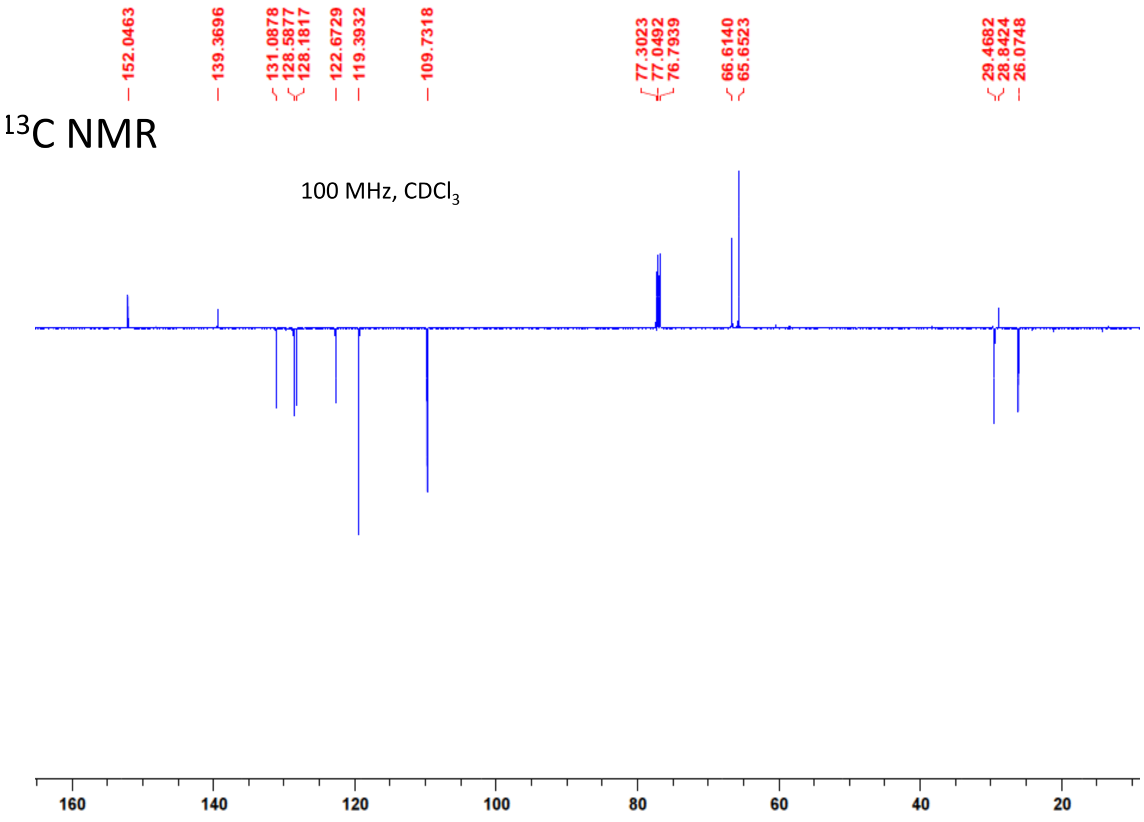
152.0463
139.3696
131.0878
128.5877
128.1817
122.6729
119.3932
109.7318
77.3023
77.0492
76.7939
66.6140
65.6523
29.4682
28.8424
26.0748
^{13}C NMR
100 MHz, $CDCl_3$
160
140
120
100
80
60
40
20

Compound **3**

^{11}B NMR

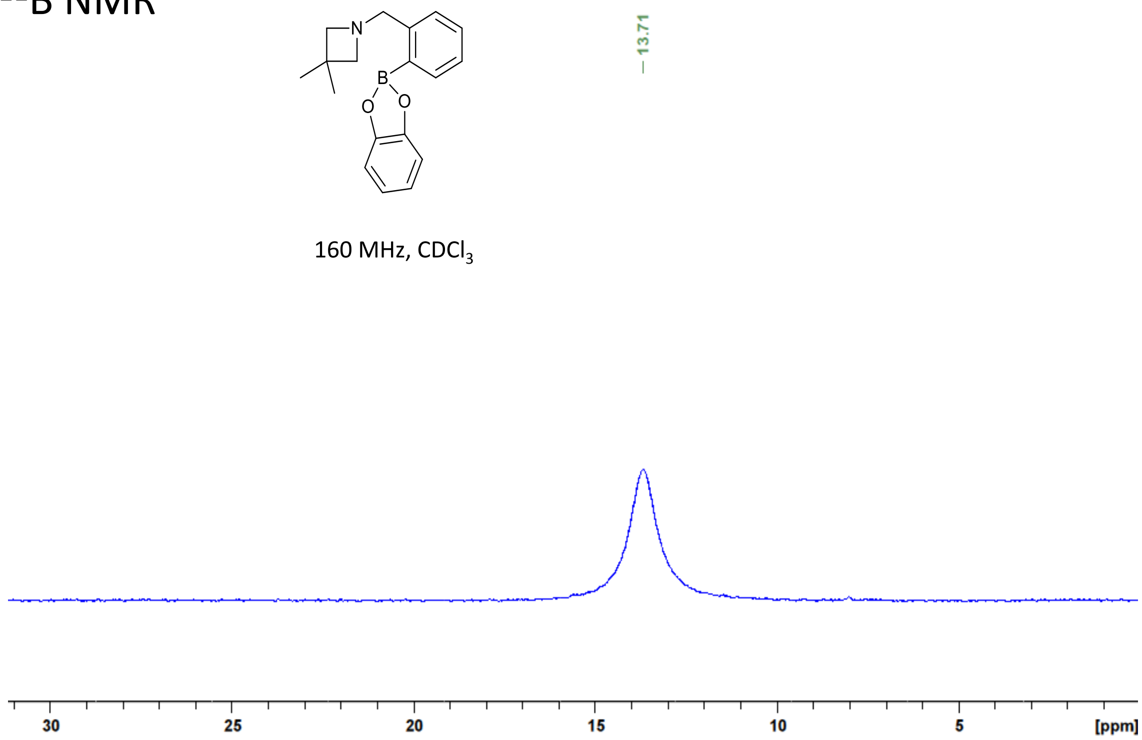

^{11}B NMR

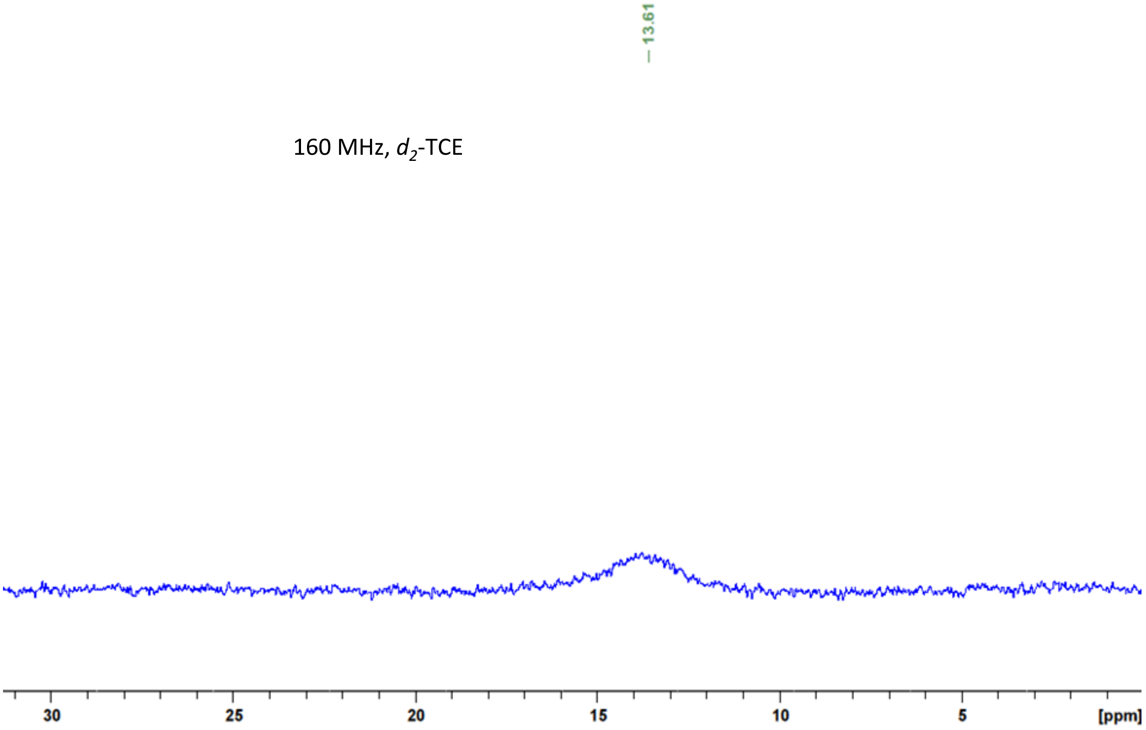

Compound **3**

^{11}B NMR

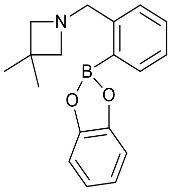

160 MHz, *d*$_5$-pyridine

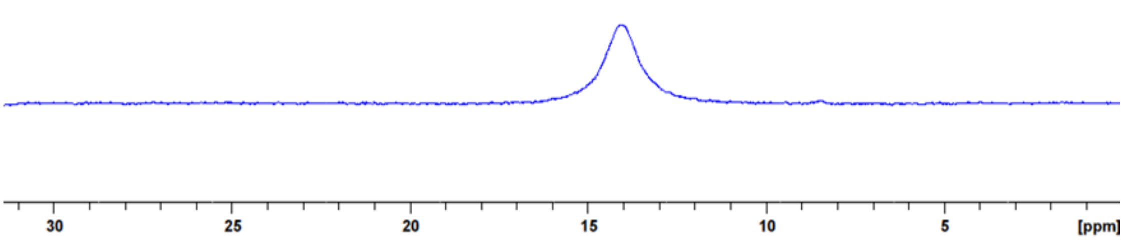

Compound **4**

^{1}H NMR

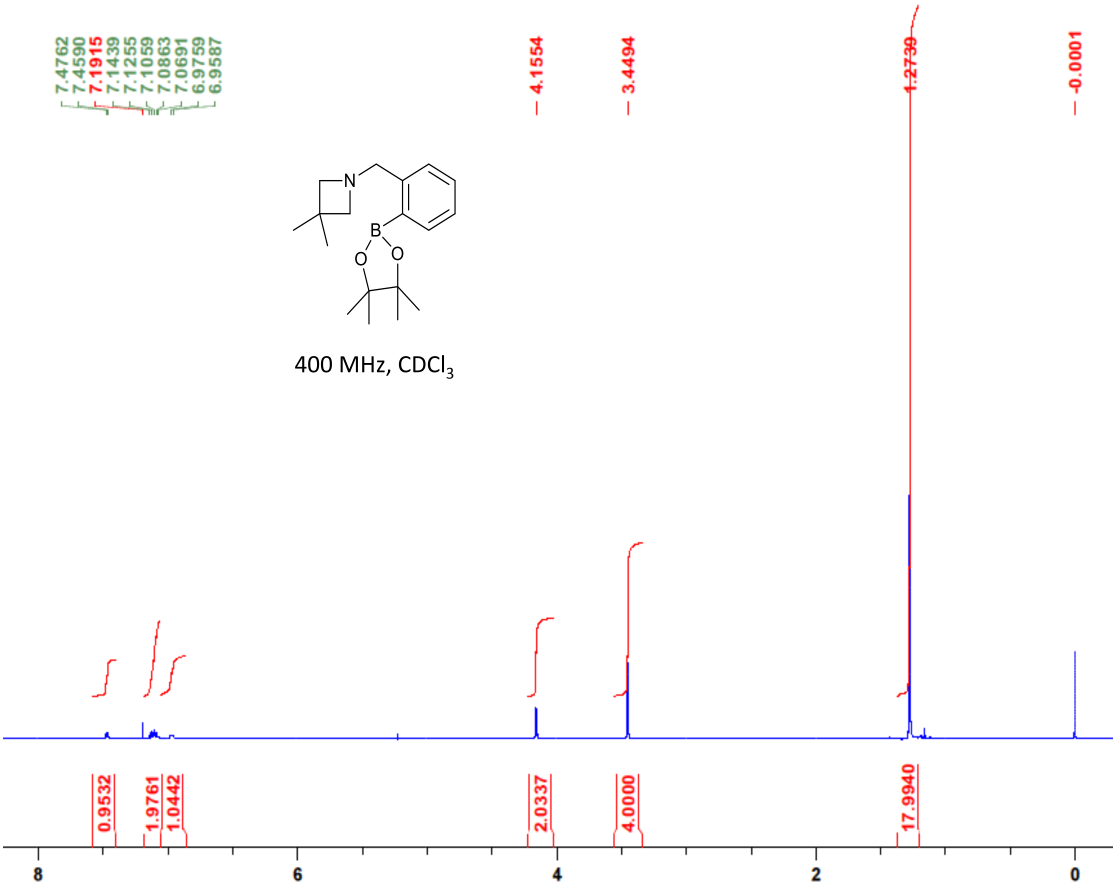

400 MHz, $CDCl_3$

^{13}C NMR

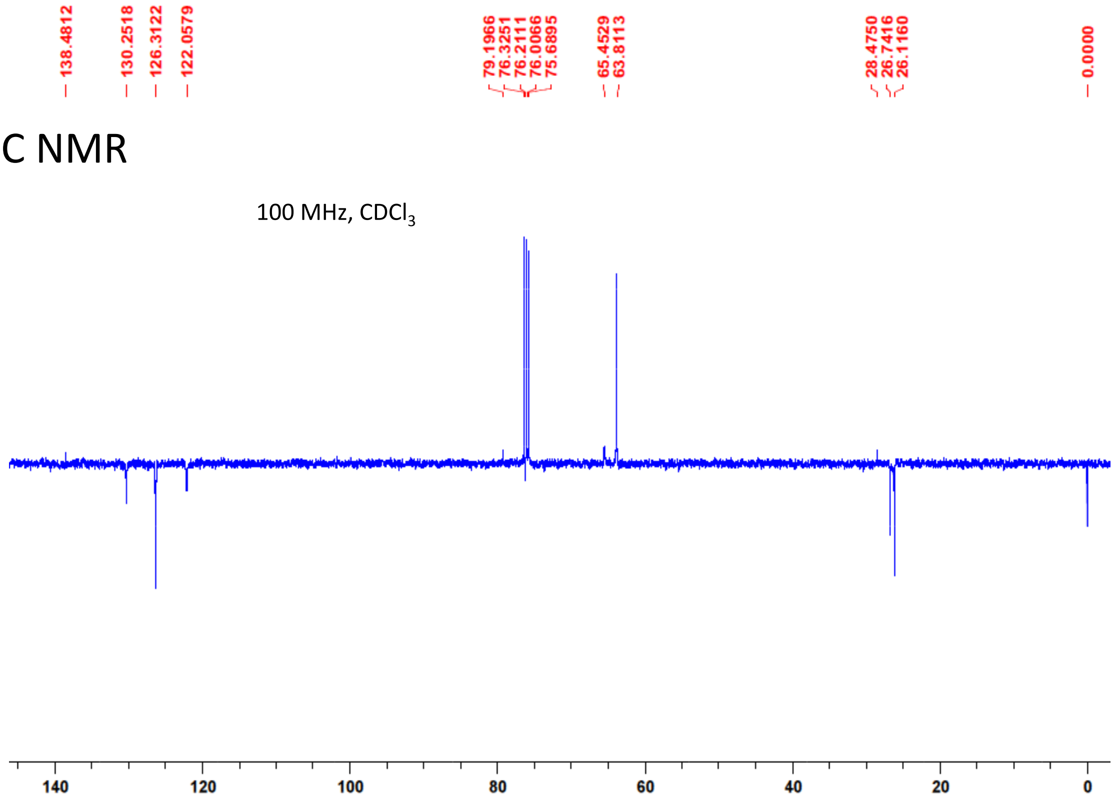

100 MHz, $CDCl_3$

Compound **4**

^{11}B NMR

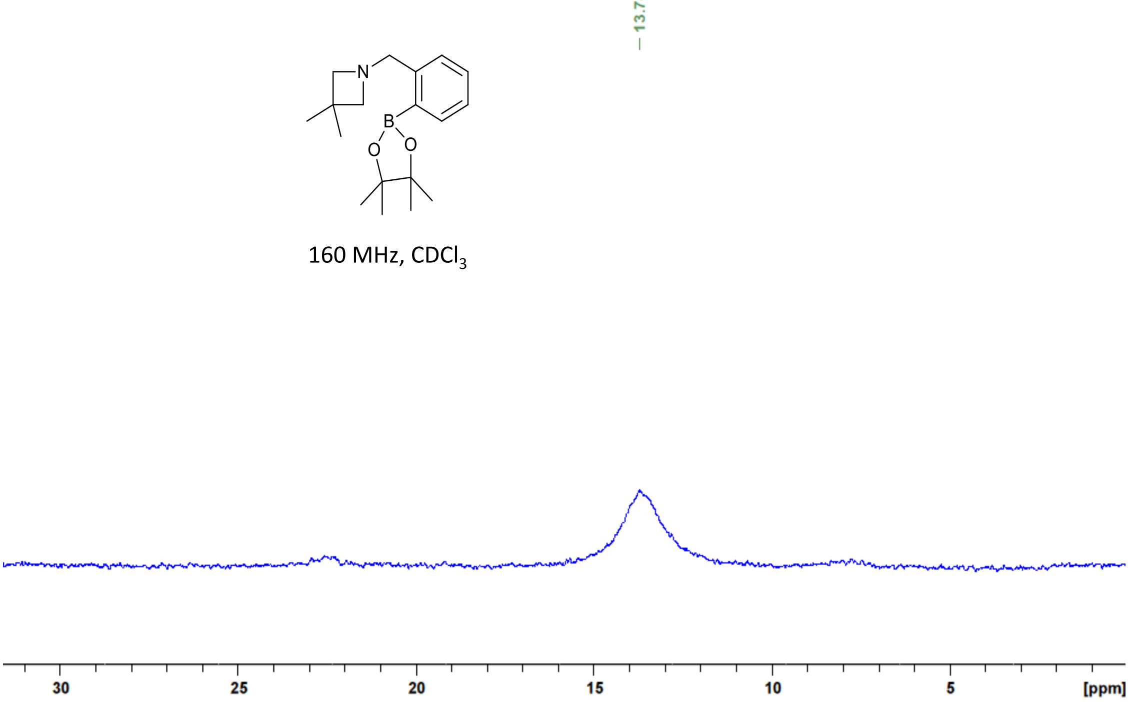

^{11}B NMR

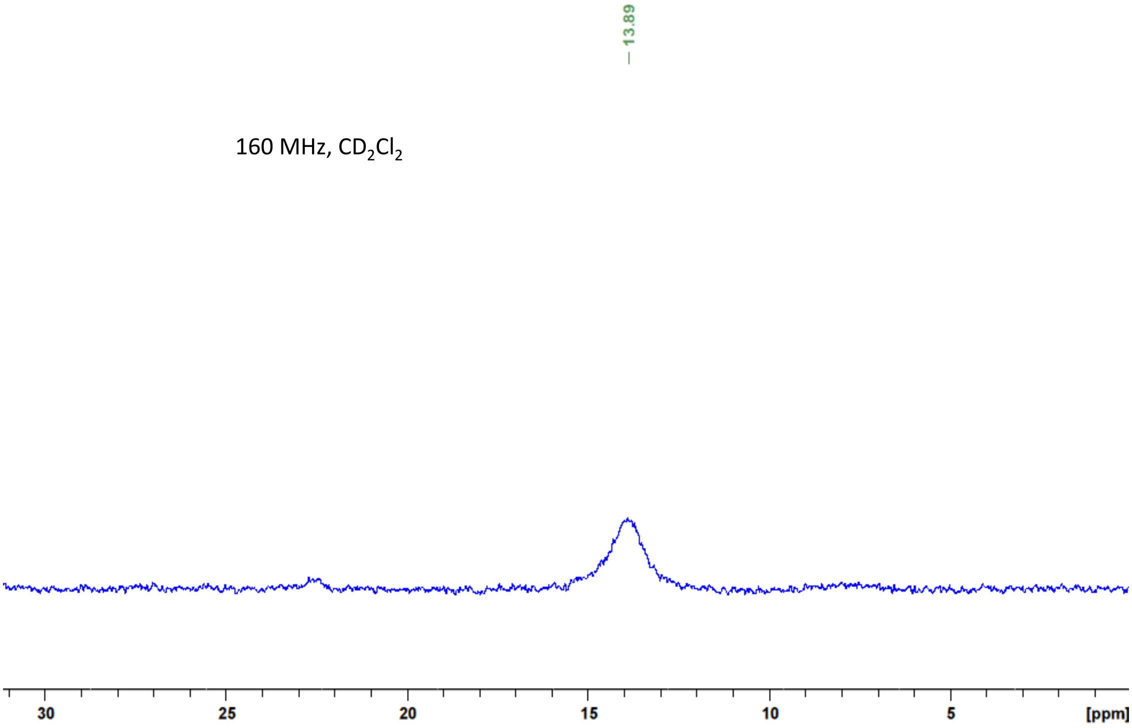

General method for the determination of activation parameters. Variable temperature NMR spectra were recorded at 500 MHz on a Bruker DRX spectrometer in 1,1,2,2-*d*$_2$-tetrachloroethane (*d*$_2$-TCE), *d*$_5$-pyridine (*d*$_5$-Py) or CD_2Cl_2. Temperature calibration of the spectrometer was performed using CH_3OH/CD_3OD (<298 K) and $HOCH_2CH_2OH$/DMSO-d_6 (>298 K).[2] Natural line widths for each spectrum were determined by line fitting deconvolution with Mestrec-Nova. The chemical shifts of the corresponding exchangeable signals at close to coalescence were determined from a plot of Δ_A-$\Delta\Delta_B$ (in Hz) vs T at temperatures well below coalescence. Simulated spectra for the A_2X_2 spin system (for compound **3** in *d*$_2$-TCE and *d*$_5$-Py, compound **4** in or CD_2Cl_2) were generated using the WINDNMR package (version 7.1.12)[3] and compared with the acquired spectra using difference spectra. From these simulations, the rate constant k for inversion could be determined as a function of temperature. Hence, from the Eyring equation, the activation parameters could be determined by plotting ln(k/T) versus 1/T wherein:

$$\Delta H^{\ddagger} = -(\text{slope})R \text{ and } \Delta S^{\ddagger} = [\text{intercept} + \ln(h/K_b)]R$$

where R = gas constant; h = Planck's constant; and k_b = Boltzmann's constant.

Variable Temperature ^{1}H NMR Spectra for 3-4:

3 in *d*$_2$-TCE:

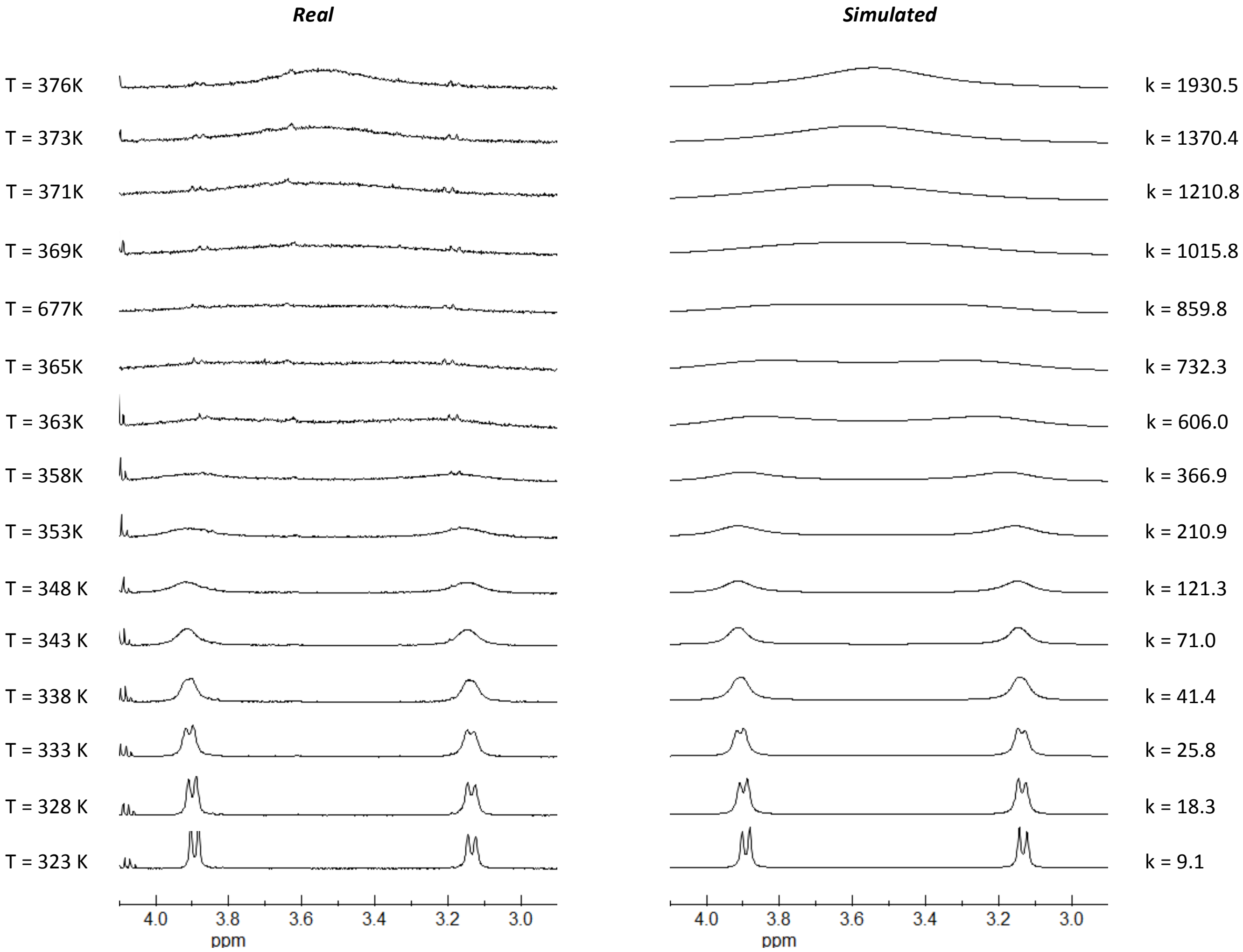

3 in d_5-Py:

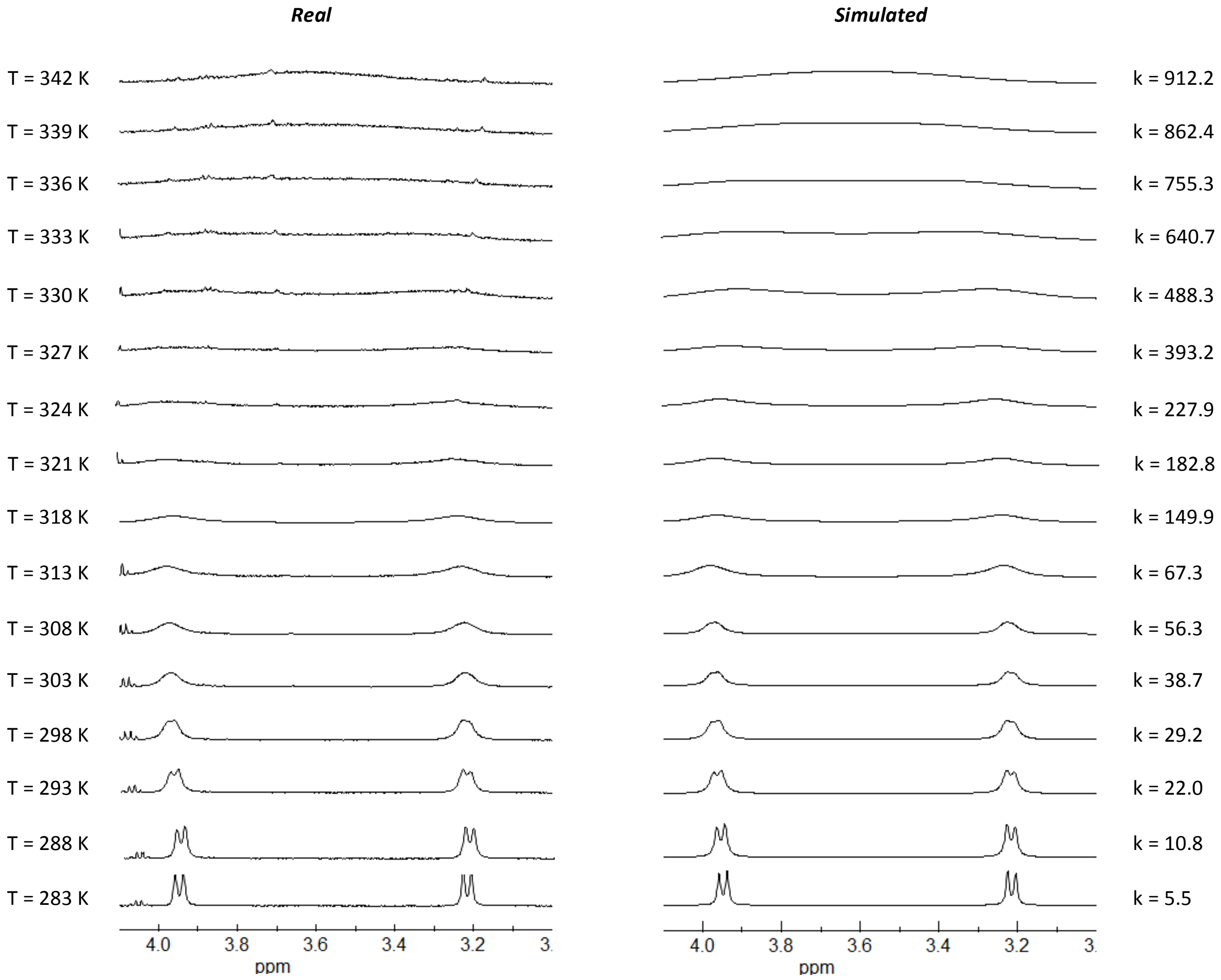
Real
Simulated
T = 342 K
T = 339 K
T = 336 K
T = 333 K
T = 330 K
T = 327 K
T = 324 K
T = 321 K
T = 318 K
T = 313 K
T = 308 K
T = 303 K
T = 298 K
T = 293 K
T = 288 K
T = 283 K
k = 912.2
k = 862.4
k = 755.3
k = 640.7
k = 488.3
k = 393.2
k = 227.9
k = 182.8
k = 149.9
k = 67.3
k = 56.3
k = 38.7
k = 29.2
k = 22.0
k = 10.8
k = 5.5
4.0
3.8
3.6
3.4
3.2
3.
ppm
4.0
3.8
3.6
3.4
3.2
3.
ppm

4 in CD_2Cl_2:

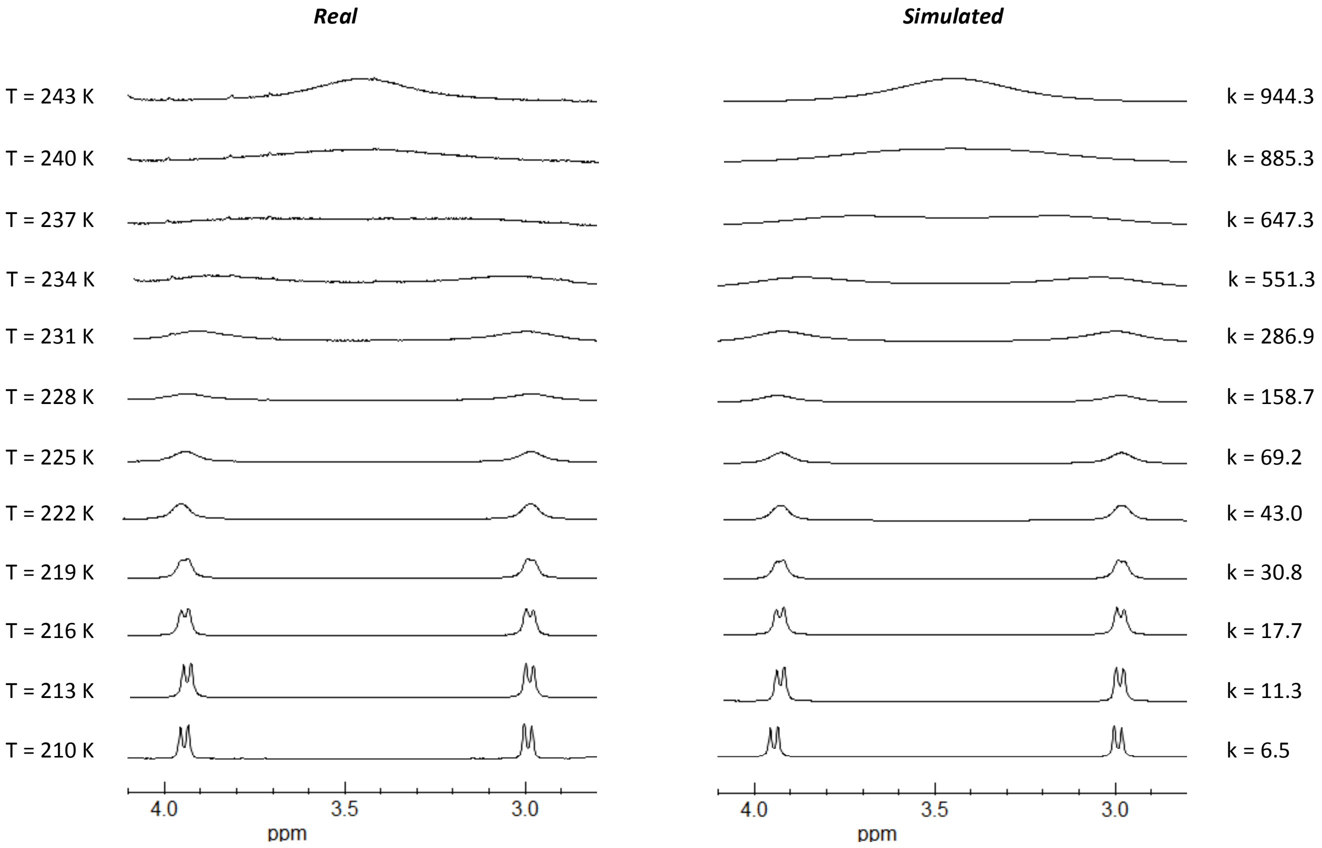
Real
Simulated
T = 243 K
T = 240 K
T = 237 K
T = 234 K
T = 231 K
T = 228 K
T = 225 K
T = 222 K
T = 219 K
T = 216 K
T = 213 K
T = 210 K
k = 944.3
k = 885.3
k = 647.3
k = 551.3
k = 286.9
k = 158.7
k = 69.2
k = 43.0
k = 30.8
k = 17.7
k = 11.3
k = 6.5
4.0
3.5
3.0
ppm
4.0
3.5
3.0
ppm

Eyring plots and activation parameters:

For **3** in *d*$_2$-TCE:

$\Delta H^\ddagger = 100.2$ kJ mol^{-1}; $\Delta S^\ddagger = 82.2$ J K^{-1} mol^{-1} and $\Delta G^\ddagger$ (at 298 K) = 75.7 kJ mol^{-1}.

T (K)	k
323	9.1
328	18.3
333	25.8
338	41.4
343	71.0
348	121.3
353	210.9
358	366.9
363	606.0
365	732.3
367	859.8
369	1015.8
371	1210.8
373	1370.4
376	1930.5

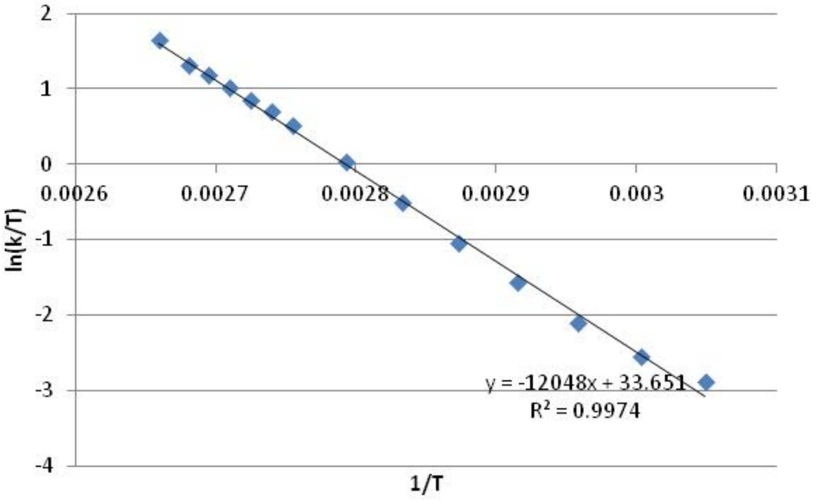

For **3** in *d*$_5$-Py:

$\Delta H^\ddagger = 67.4$ kJ mol^{-1}; $\Delta S^\ddagger = 8.7$ J K^{-1} mol^{-1} and $\Delta G^\ddagger$ (at 298 K) = 64.8 kJ mol^{-1}.

T (K)	k
283	5.5
288	10.8
293	22.0
298	29.2
303	38.7
308	56.3
313	67.3
318	149.9
321	182.8
324	227.9
327	393.2
330	488.3
333	640.7
336	755.3
339	862.4
342	912.2

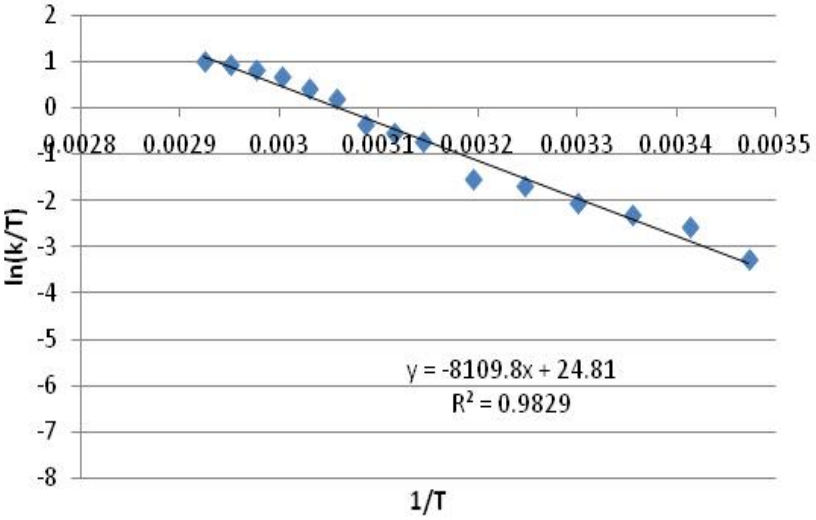

For **4** in CD_2Cl_2:

$\Delta H^{\ddagger} = 67.6$ kJ mol^{-1}; $\Delta S^{\ddagger} = 95.0$ J K^{-1} mol^{-1} and $\Delta G^{\ddagger}$ (at 298 K) = 39.3 kJ mol^{-1}.

T (K)	k
210	6.5
213	11.3
216	17.7
219	30.8
222	43.0
225	69.2
228	158.7
231	286.9
234	551.3
237	647.3
240	885.3
243	944.3

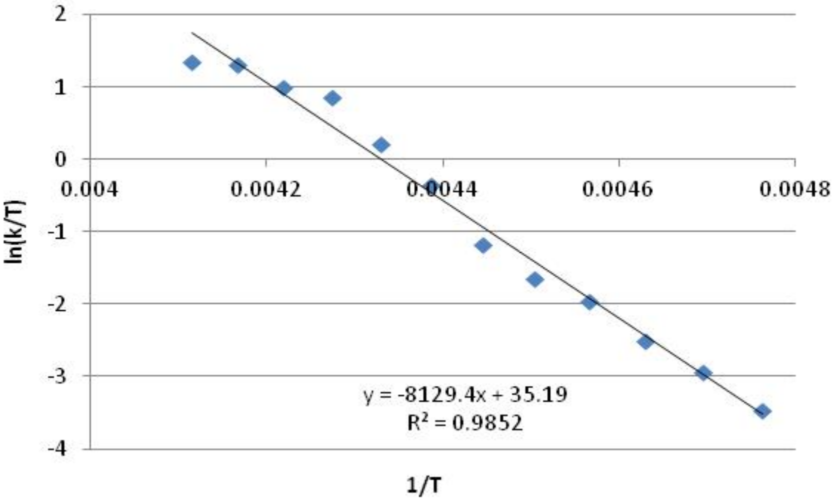

Computational Modelling of 1, 3 and 4

Inversion Barrier Calculations: All first-principles calculations were performed using the GAUSSIAN09 package.[4] Since the barriers should at least in part be affected by non-bonded interactions, an approach that can recover such interactions, such as Møller-Plesset 2nd order perturbation theory (MP2) is preferable. Here, we have tested the performance of density functional theory (DFT) against MP2 theory in this respect, via use of the PBE1PBE hybrid exchange-correlation functional.[5]

DFT Calculations: All six structures [one minimum and one transition state each for **1**, **3** and **4**] were first optimized in the gas-phase at the PBE1PBE/6-31G* level of theory.

We performed systematic searches over possible ground state (GS) structures by considering the range of rotamers supported by these compounds. For each compound there are only a few rotable bonds; we have explored the possible rotatmers by generating initial structures with systematic increments in the torsional angles defined over the atoms C-B-O-C and C-N-C-C(Ar). For each set of possible torsional angles, we performed a geometry optimization calculation. The GS structures reported represent the lowest-energy structures identified from this procedure (and then subsequently refined as detailed below). Alternative structures were at least 30 kJ mol^{-1} higher in energy than those reported here.

Similarly, we performed a thorough rotameric search for the possible transition state (TS) structures. While we explored a range of transition-state structures, only two such TSs corresponded with pyramidal nitrogen inversion. The TS structures reported correspond with the nitrogen-inversion TS of lowest energy. Again, these structures formed the basis for subsequent refinement as described below.

For each of these structures, the geometry was re-optimized in the presence of an implicit solvent, using the polarizable continuum model (PCM) of Tomasi and co-workers.[6] The implicit solvation model was configured in GAUSSIAN09 to model toluene, so as to represent a general non-polar solvent. Analytic 2nd-derivatives were calculated in the implicit solvation runs to check the character of each stationary point, in particular confirming that all transition-states corresponded to first-order saddles on the potential energy surface. In each case, the transition vectors were inspected to confirm the mechanism of interconversion. Harmonic frequencies were subsequently used to estimate the change in Gibbs free energy between each pair of minimum and transition-state. In this way, the following Gibbs free energy barriers were obtained: **1**: 24.8 kJ mol^{-1}; **3**: 56.6 kJ mol^{-1}; and **4**: 12.7 kJ mol^{-1}.

MP2 Calculations: Using the optimised PBE1PBE geometries from the implicit solvent calculations, we calculated single-point energies in the implicit solvent at the MP2/aug-cc-pVDZ level of theory. For each of these structures, we added on the free energy thermal corrections obtained from the corresponding PBE1PBE calculation. In this way we obtained

Gibbs free energy barriers for the 3 structures in implicit toluene solvent: **1**: 35.4 kJ mol^{-1}; **3**: 111.4 kJ mol^{-1}; and **4**: 67.2 kJ mol^{-1}.

Secondary-hydrogen bonding: We exclude the possibility of secondary hydrogen-bonding making a significant contribution to the free energy associated with nitrogen pyramidal inversion, based on the structural evidence given below. Specifically, we consider the O…N non-bonded distances, O…C non-bonded distances, and the O…C-H angles in the ground state structure for both compounds **3** and **4**. We report the O…C distances and related angles for both the closest azetidine methyl group, as well as the two azetidine methylene groups. In the case of the experimentally determined structure (**3**), where there exist two structures in the unit cell, we provide data for the second structure in parentheses.

	3 **Calculated**	**3** **Experiment**	**4** **Calculated**
O…N distance / Å	2.59/2.53	2.57/2.54 (2.58/2.53)	2.59/2.57
O…C methyl distance / Å[a]	3.55	3.46 (3.60)	3.44
O…C-H methyl angle / °	35	33 (33)	31
O…C distance / Å[b]	2.91/3.01	2.90/3.01 (2.90/2.99)	2.93/3.17
O…C-H methylene angle / °	51/57	53/59 (52/59)	53/61

[a] Between oxygen atom and azetidine methyl group in closest proximity. [b] Distance from each oxygen atom of the boronate ester to its nearest azetidine CH_2 neighbour.

In the case of the O…C methyl contacts, the carbon atom is too distant to make a significant contribution to a hydrogen-bond. In the case of the O…C methylene contacts, while some of the O…C distances could plausibly support a hydrogen-bond, the O…C-H angles clearly show that hydrogen-bonds are not possible given the orientation of the CH bonds.

Natural Bonding Orbital (NBO) analysis: To gain a deeper insight into the electronic properties of the B…N and related interactions, we carried out a natural bond orbital (NBO) population analysis[7] at the PBE1PBE/6-31G* level of theory for the GS structures of **3** and **4**.

The delocalization of electron density from the nitrogen lone-pair to the boron 2*p* orbital stabilizes the donor-acceptor interaction. The corresponding second-order perturbation theory analyses of the Kohn-Sham equations indicate a stabilization energy of 112 vs 88 kJ mol^{-1} (for **3** and **4** respectively) supporting a stronger B–N bond in **3**.

In a similar vein, the calculated stabilization energy associated with delocalization of electron density from each oxygen lone-pair to the boron 2*p* orbital is more pronounced for **4** compared with **3** (225 vs 211 kJ mol^{-1} for oxygen 1, and 232 vs 221 kJ mol^{-1} for oxygen 2, for **4** and **3** respectively), suggesting that increased levels of back-donation and overlap between the oxygen lone-pairs and boron in **4** compared with **3**.

Optimised Ground State (GS) and Transition State (TS) geometries for 1, 3 and 4.

GS1:

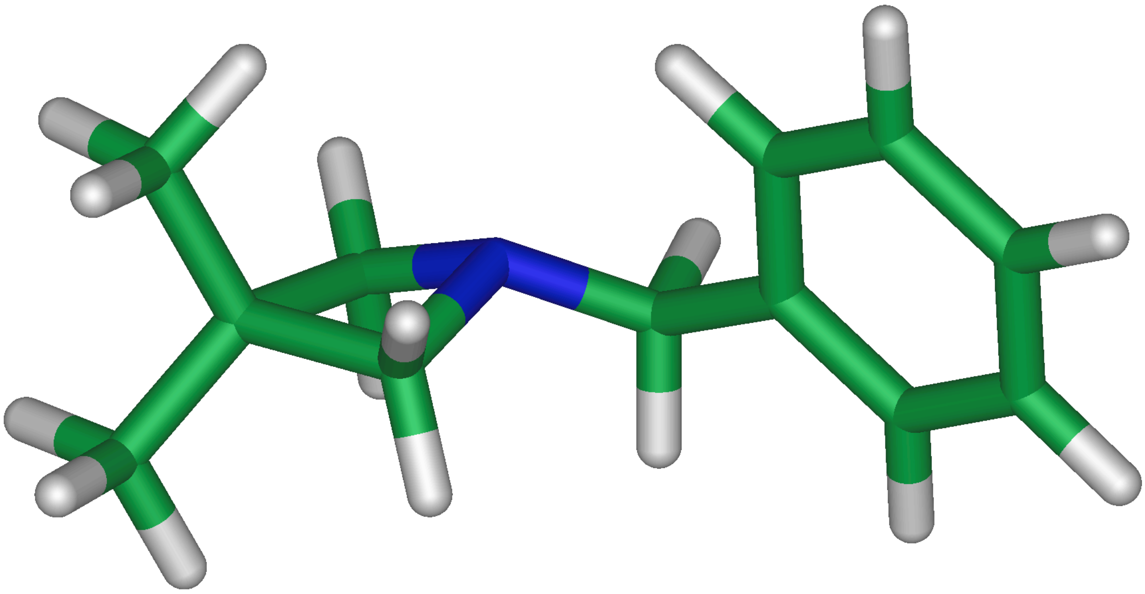

TS1

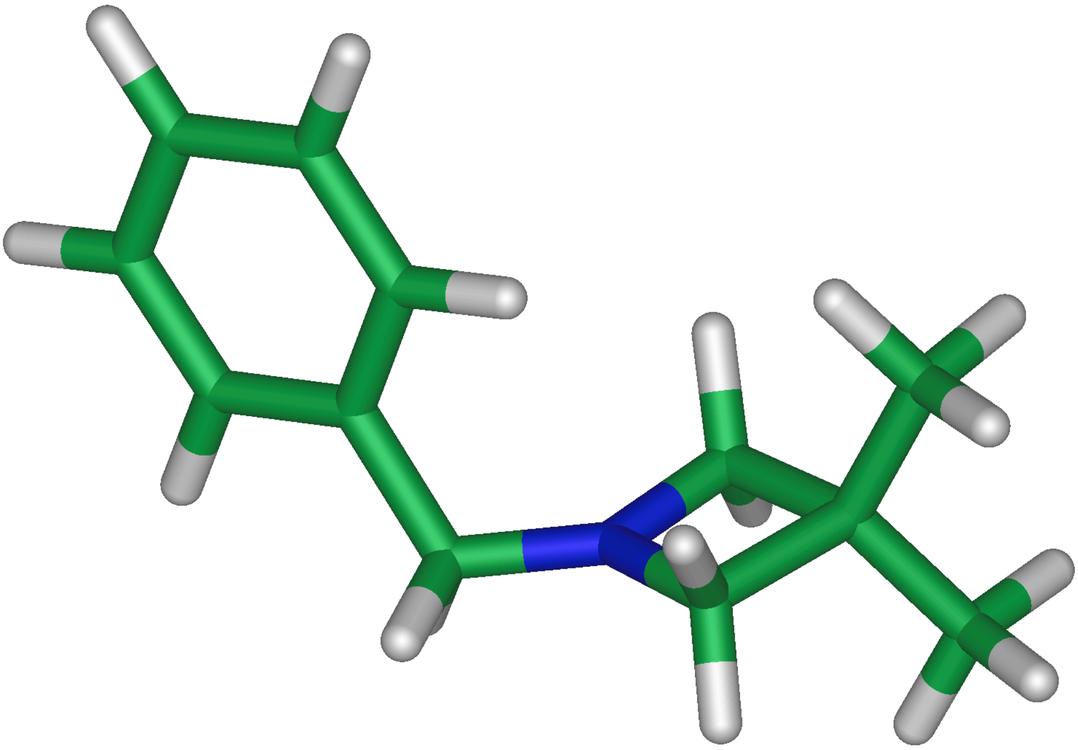

GS3:

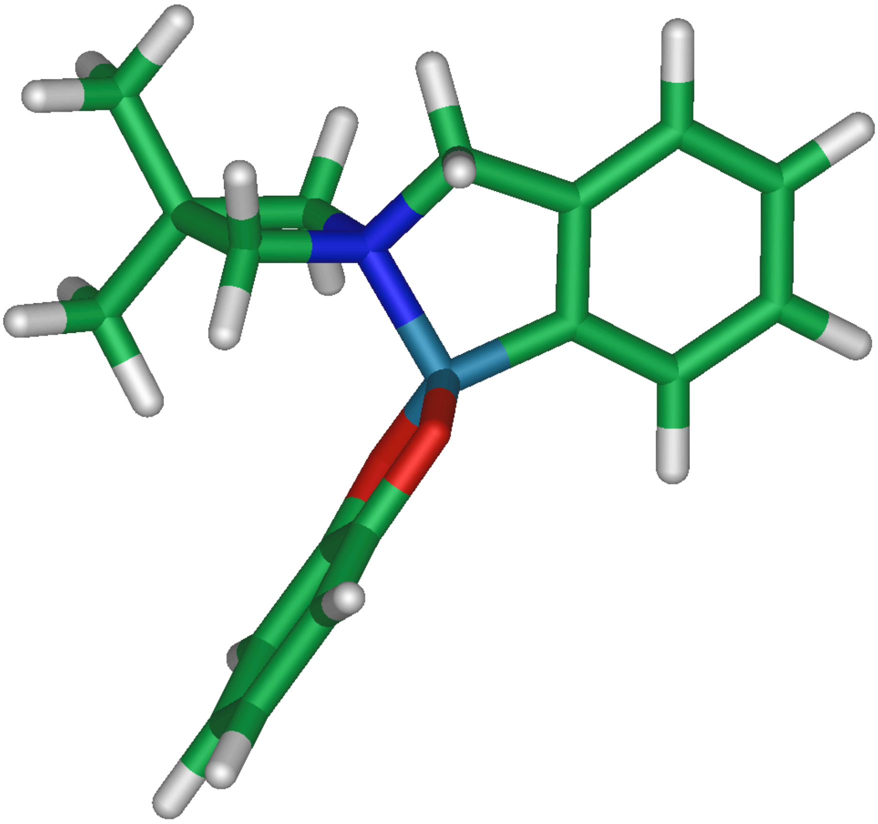

TS3:

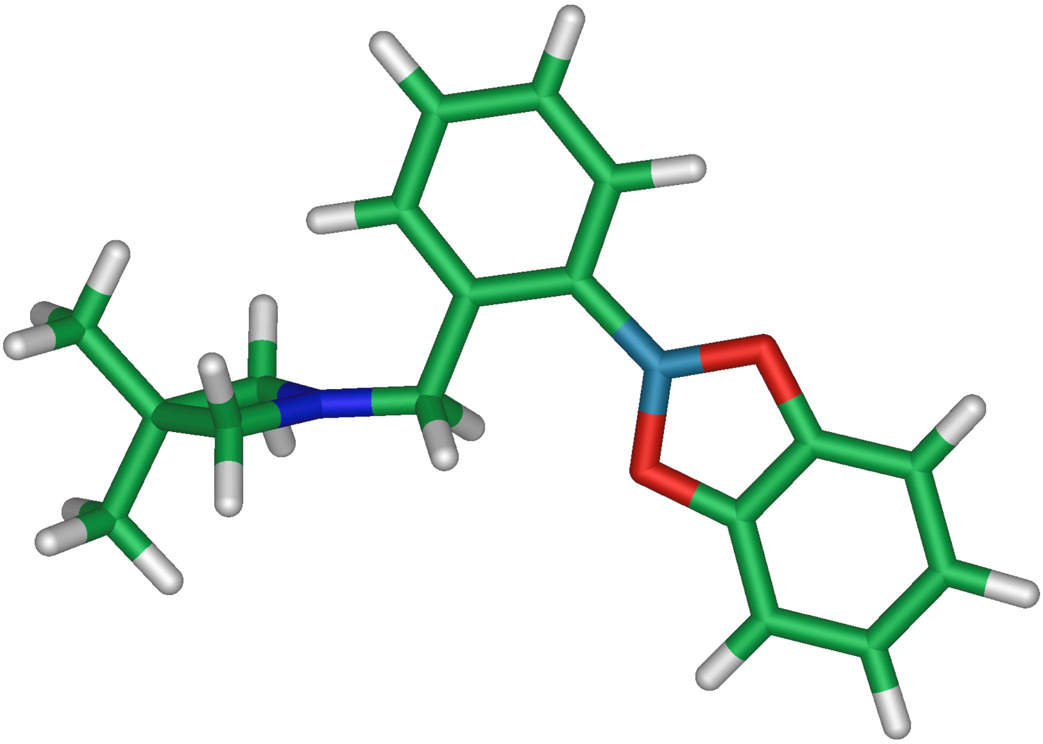

GS4:

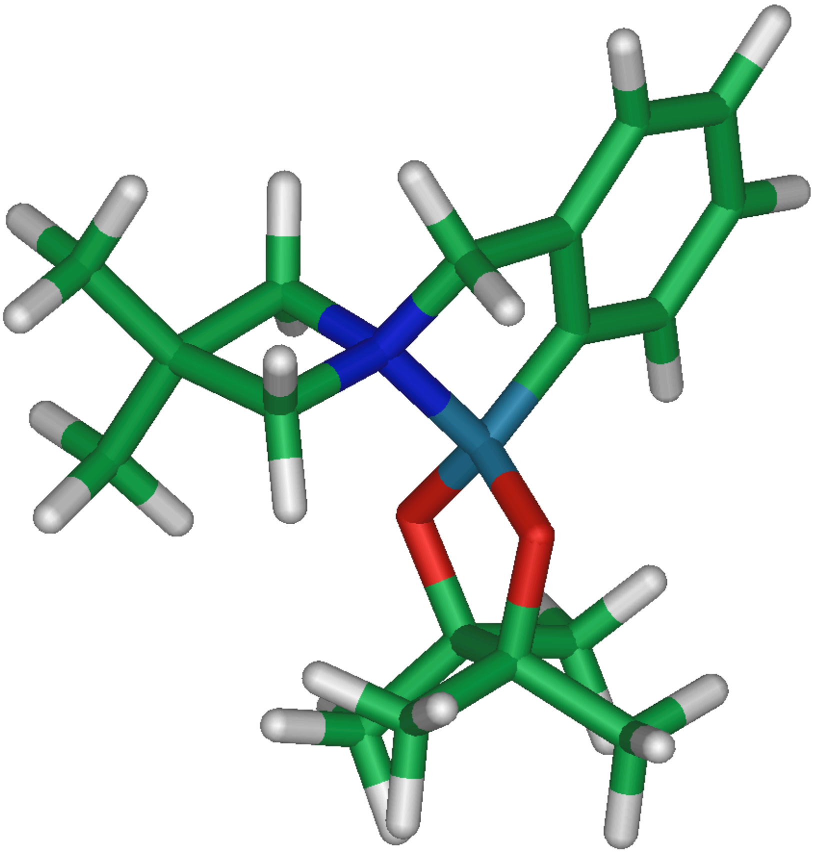

TS4:

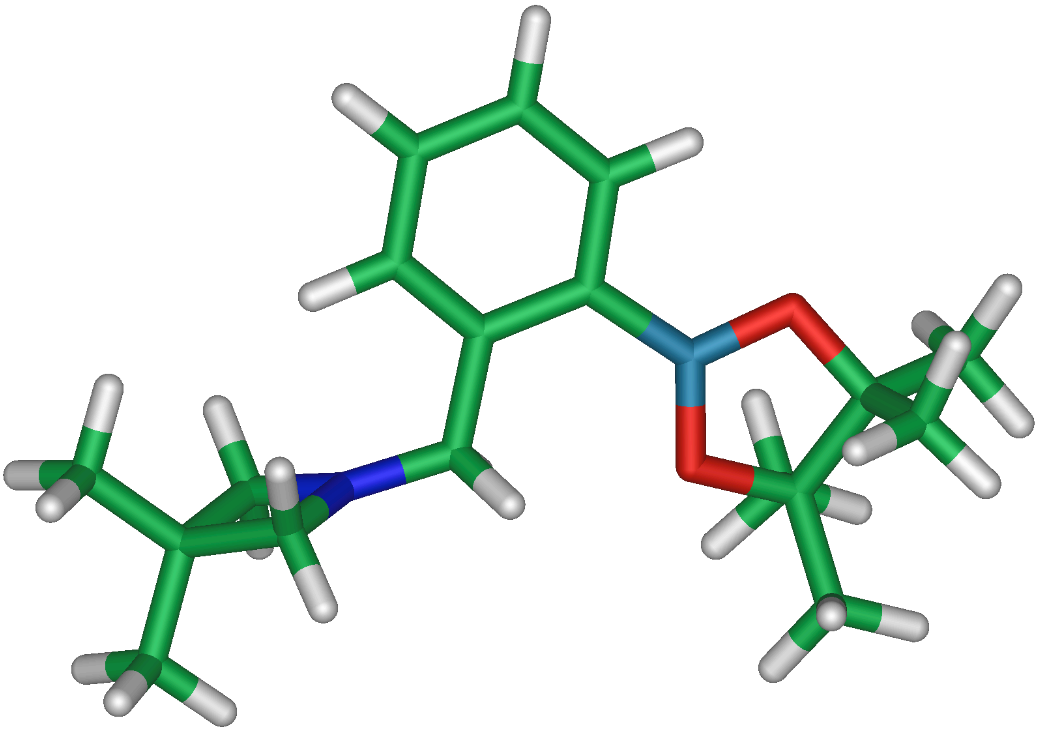

X-ray structure of 3 (CCDC 894158).

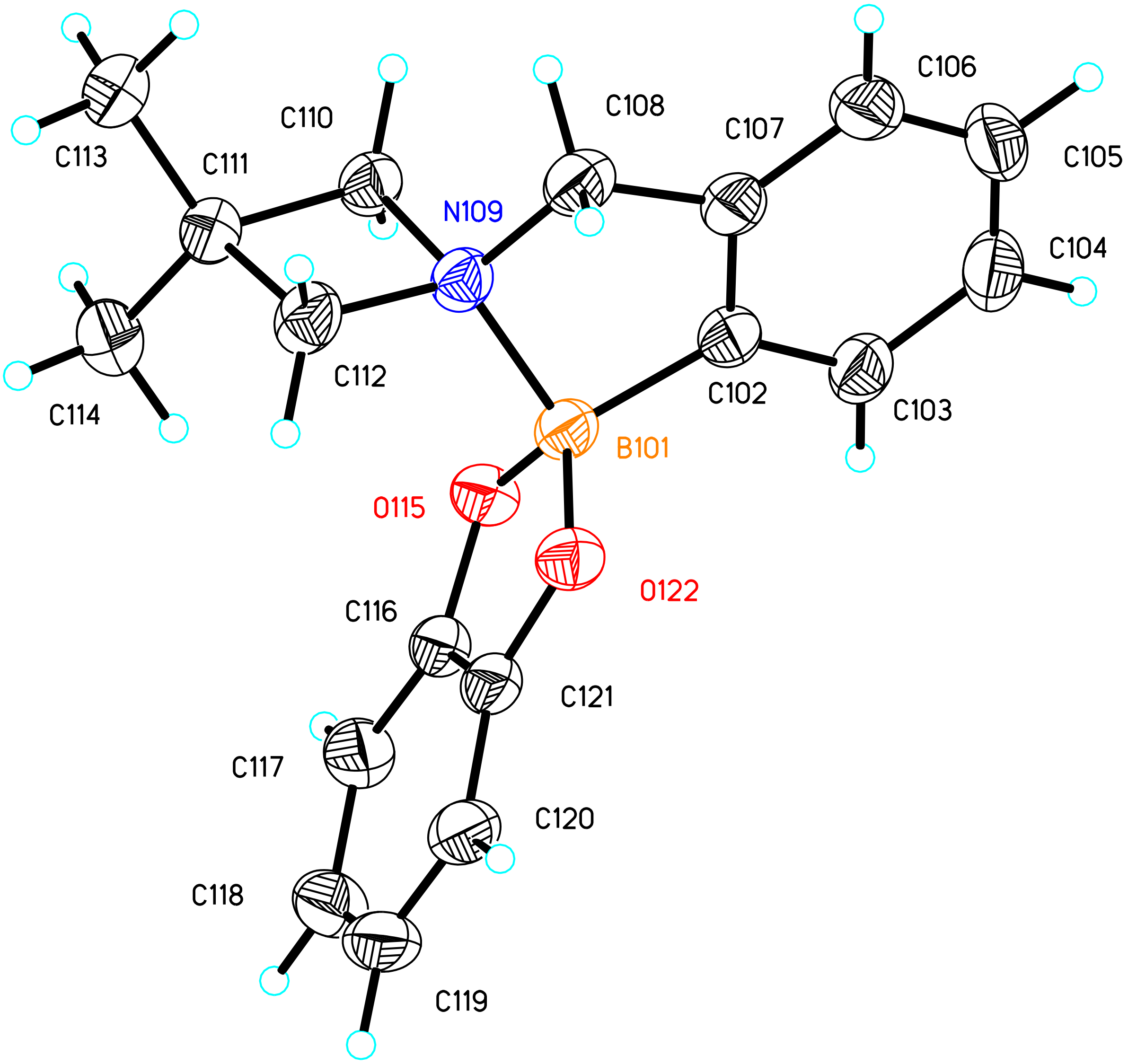

Solid-state structure and atom numbering of one of the crystallographically independent but chemically equivalent molecules in **3.** Thermal ellipsoids at 50% probability.

Overlay of computed (orange) and solid-state structure (green) of 3:

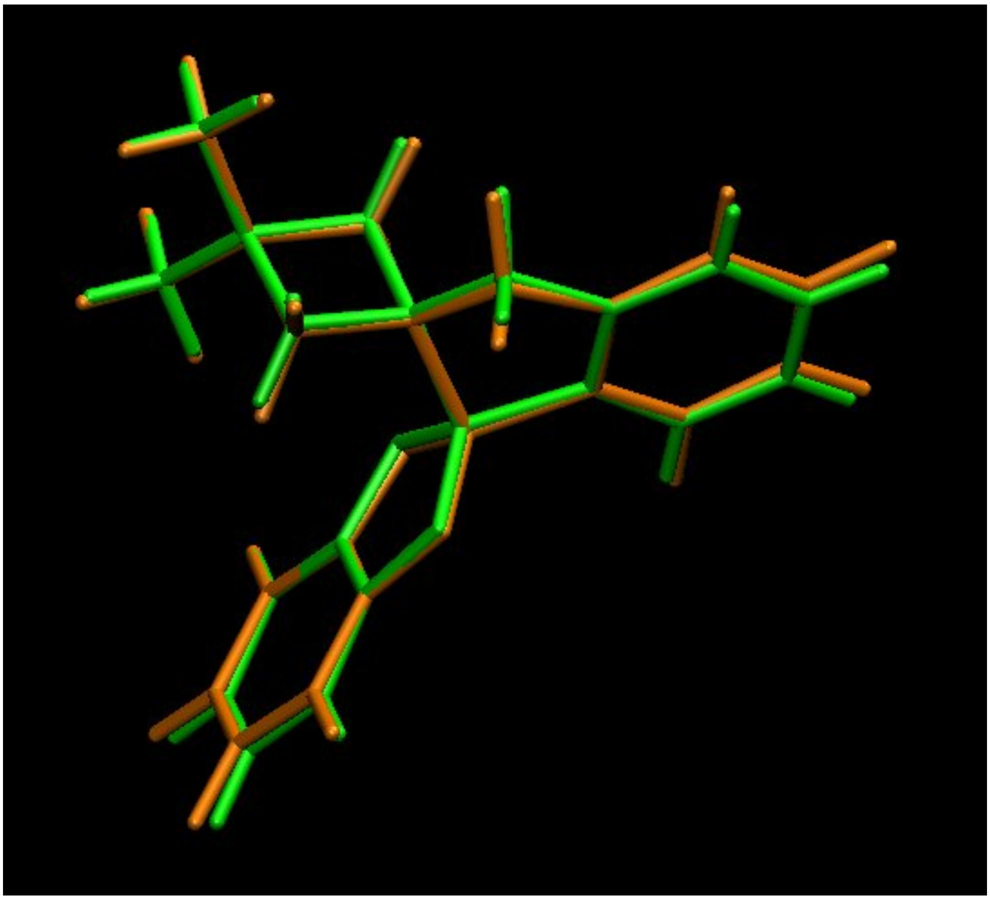

References:

[1] H. W. Thompson and J. Swistok, *J. Org. Chem.* 1981, **46**, 4907.

[2] S. Berger, S. Braun, *200 and More NMR Experiments A Practical Course*, Chapter 5, Wiley-VCH, **2004**.

[3] H. J. Reich, "WinDNMR: Dynamic NMR Spectra for Windows." *J. Chem. Educ. Software*, **1996**, 3D, 2.

[4] Gaussian 09, Revision A.1, M. J. Frisch, G. W. Trucks, H. B. Schlegel, G. E. Scuseria, M. A. Robb, J. R. Cheeseman, G. Scalmani, V. Barone, B. Mennucci, G. A. Petersson, H. Nakatsuji, M. Caricato, X. Li, H. P. Hratchian, A. F. Izmaylov, J. Bloino, G. Zheng, J. L. Sonnenberg, M. Hada, M. Ehara, K. Toyota, R. Fukuda, J. Hasegawa, M. Ishida, T. Nakajima, Y. Honda, O. Kitao, H. Nakai, T. Vreven, J. A. Montgomery, Jr., J. E. Peralta, F. Ogliaro, M. Bearpark, J. J. Heyd, E. Brothers, K. N. Kudin, V. N. Staroverov, R. Kobayashi, J. Normand, K. Raghavachari, A. Rendell, J. C. Burant, S. S. Iyengar, J. Tomasi, M. Cossi, N. Rega, J. M. Millam, M. Klene, J. E. Knox, J. B. Cross, V. Bakken, C. Adamo, J. Jaramillo, R. Gomperts, R. E. Stratmann, O. Yazyev, A. J. Austin, R. Cammi, C. Pomelli, J. W. Ochterski, R. L. Martin, K. Morokuma, V. G. Zakrzewski, G. A. Voth, P. Salvador, J. J. Dannenberg, S. Dapprich, A. D. Daniels, Ö. Farkas, J. B. Foresman, J. V. Ortiz, J. Cioslowski, and D. J. Fox, Gaussian, Inc., Wallingford CT, 2009.

[5] P. Perdew, K. Burke, and M. Ernzerhof, "Errata: Generalized gradient approximation made simple," *Phys. Rev. Lett.*, **78** (1997) 1396; J. P. Perdew, K. Burke, and M. Ernzerhof, "Errata: Generalized gradient approximation made simple," *Phys. Rev. Lett.*, **78** (1997) 1396.

[6] M. T. Cancès, B. Mennucci, and J. Tomasi, *J. Chem. Phys.* 1997, **107**, 3032; M. Cossi, V. Barone, B. Mennucci, and J. Tomasi, *Chem. Phys. Lett.* 1998, **286**, 253; B. Mennucci, J. Tomasi, *J. Chem. Phys.* 1997, **106**, 5151.

[7] J. P. Foster and F. Weinhold, *J. Am. Chem. Soc.*, 1980, **102**, 7211.